The 8th European Congress on Computational Methods in Applied Sciences and Engineering
ECCOMAS Congress 2022
5-–9 June 2022, Oslo, Norway

SINGLE EDGE NOTCHED TENSION TESTING FOR ASSESSING HYDROGEN EMBRITTLEMENT: A NUMERICAL STUDY OF TEST PARAMETER INFLUENCES ECCOMAS CONGRESS 2022

ROBIN DEPRAETERE[1], WIM DE WAELE[1], MARGO CAUWELS[2], TOM DEPOVER[2], KIM VERBEKEN[2], STIJN HERTELÉ[1]

[1] Department of Electromechanical, Systems and Metal Engineering
Soete Laboratory, Ghent University
Technologiepark-Zwijnaarde 46, 9052 Zwijnaarde, Belgium

[2] Department of Materials, Textiles and Chemical Engineering
Sustainable Materials Science, Ghent University
Technologiepark-Zwijnaarde 46, 9052 Zwijnaarde, Belgium

Key words: Hydrogen Embrittlement, Fracture Toughness Testing, Finite Element Method, Continuum Damage Modelling, Diffusion

Abstract. To evaluate the feasibility of the safe use of existing gas grids for the transport and storage of hydrogen gas, the phenomenon of hydrogen assisted degradation of steel used in the pipeline grid has to be examined. A finite element based framework developed for describing this phenomenon at the continuum scale is used to assist in the design and analysis of experimental characterisation of the tearing resistance. The framework is based on the complete Gurson model for ductile damage and takes into account damage acceleration due to the local hydrogen concentration, and the diffusion of hydrogen. Simulations representing single edge notched tension (SENT) fracture toughness tests of an API 5L X70 grade steel are performed and results are discussed in terms of crack growth resistance curves. Side grooves are included in the geometry of the SENT model to promote uniform crack growth. Different boundary conditions are employed, simulating ex-situ and in-situ hydrogen charging of specimens. Moreover, the effect of the applied deformation rate on the dynamics of hydrogen diffusion and the resulting toughness values is investigated. Accordingly, guidance regarding experimental SENT testing for the hydrogen assisted tearing resistance degradation is provided, in terms of test conditions (in-situ/ex-situ) and deformation rate.

1 INTRODUCTION

Hydrogen will play a key role in the future low-carbon society. One of the challenges in transporting hydrogen gas through steel pipelines is the well-acknowledged reduction in the mechanical properties of steel, also known as hydrogen embrittlement (HE). As for now, qualification of the pipeline steel for hydrogen use requires significant safety factors on the maximum allowable operating pressure, or expensive mechanical testing, as e.g. prescribed by ASME B31.12 [1].

Furthermore, the specific mechanisms governing HE are still debated [2], and multiple theories have been proposed [3].

The development of numerical models describing HE can aid in the analysis of the mechanical tests, increase the understanding of HE and thus allow to predict the effect of certain influencing parameters on the mechanical properties. Accurate numerical modelling of HE requires a multi-physics approach coupling the reduction in mechanical properties to the hydrogen diffusion [4]. The diffusion of hydrogen atoms is derived by Krom et al. [5], and includes the stress-assisted diffusion towards regions of high hydrostatic stress. The mechanistic effect of the hydrogen atoms is debated, since it depends on the assumed theory. On the one hand, Hydrogen Enhanced DEcohesion (HEDE) assumes that the interatomic binding strength in the lattice is reduced due to hydrogen. On the other hand, theories exist that start from the dominance of plasticity such as Hydrogen Enhanced Localized Plasticity (HELP) describing the accelerated plasticity due to hydrogen atoms, and Hydrogen Enhanced Strain-Induced Vacancy (HESIV) where the hydrogen promotes the formation of vacancies upon straining [3]. Whereas continuum-scale models describing HEDE are well employed, numerical models assuming HELP and/or HESIV are lacking [6]. Recently, there have been advances in the numerical modelling of HELP and HESIV by starting from a Gurson type damage model, and rationalizing that the parameters describing the damage processes such as void nucleation, void growth and void coalescence should be adapted to account for the accelerated development of damage due to hydrogen [6, 7, 8]. It is important to stress that an accurate numerical model should make the accelerated degradation dependent on the local hydrogen concentration that varies in time and space, rather than prescribing the amount of degradation as a constant, as was carried out in previous studies [9, 10].

Regarding the transport of hydrogen through pipeline steel, the reduction in fracture toughness is of particular concern, since this may result in reduced tolerable defect sizes. The SENT fracture toughness test is relevant for thin-walled applications such as pipelines due to its comparable constraint at the crack tip [11]. In mechanical testing of hydrogenated specimens, two hydrogen charging conditions are possible: ex-situ and in-situ. Ex-situ refers to the precharging of the specimen, after which the specimen is mechanically loaded in air. On the contrary, during in-situ testing, the loading of the specimen also occurs in a hydrogen containing environment. In-situ testing is clearly more representative of the actual scenario, however it is more complex with respect to the instrumentation of the experiment.

In the present work, SENT fracture toughness tests on hydrogen-charged specimens are simulated, and the resulting crack growth resistance curves are evaluated. Both ex-situ and in-situ hydrogen charging is simulated by employing different boundary conditions. Since the response of the experiment is time-dependent due to the diffusion kinetics of hydrogen, different displacement speeds are simulated as well.

2 NUMERICAL MODELLING OF HYDROGEN-ASSISTED DEGRADATION

2.1 Hydrogen diffusion

Since the accelerated development of damage is dependent on the local hydrogen concentration, the diffusion of hydrogen atoms is an important aspect of a numerical model describing HE. The derivation by Krom et al. [5] is commonly employed:

$$\frac{C_L + C_T(1 - C_T/N_T)}{C_L}\frac{\partial C_L}{\partial t} - \nabla\cdot(D_L\nabla C_L) + \nabla\cdot\left(\frac{D_L C_L \bar{V}_H}{RT}\nabla\sigma_h\right) + \alpha\theta_T\frac{dN_T}{d\epsilon_p}\frac{\partial\epsilon_p}{\partial t} = 0 \qquad (1)$$

This equation takes into account the division of the hydrogen atoms into lattice sites (C_L in wppm) and trapping sites (C_T in wppm). The speed of the hydrogen diffusion is governed by the diffusion coefficient D_L, and the equation includes diffusion towards regions of higher hydrostatic stress σ_h. A finite element implementation for three-dimensional hydrogen diffusion using Abaqus subroutines is given in Depraetere et al. [7]. For the other parameters, reference is made to the original work by Krom et al. [5].

2.2 Damage model

The numerical framework is based on the Complete Gurson Model (CGM) [12], describing the three stages of ductile damage: void nucleation, growth and coalescence. Upon plastic deformation, the void volume fraction f increases, leading to softening and eventually failure of the element. The yield criterion is given by:

$$\phi(\boldsymbol{\sigma}, \bar{\sigma}, f^*) = \left(\frac{\sigma_e}{\bar{\sigma}}\right)^2 + 2q_1 f^* \cosh\left(\frac{3q_2\sigma_h}{2\bar{\sigma}}\right) - 1 - q_1^2 f^{*2} = 0 \qquad (2)$$

with $\boldsymbol{\sigma}$ the stress tensor, $\bar{\sigma}$ the flow stress, f^* the effective void volume fraction, σ_e the von Mises stress, σ_h the hydrostatic stress, and q_1, q_2 empirical constants. The effective void volume fraction f^* is related to the real void volume fraction f but is accelerated upon coalescence. Upon reaching the final void volume fraction f_f, complete failure of the element is assumed and all load-carrying capacity is lost. An initial void volume fraction f_0 is assumed.

Void nucleation and void growth cause the evolution of the void volume fraction f:

$$\dot{f} = \dot{f}_{growth} + \dot{f}_{nucleation} \qquad (3)$$

Void nucleation is typically described by the strain-controlled approach by Chu and Needleman [13]:

$$\dot{f}_{nucleation} = \frac{f_N}{s_N\sqrt{2\pi}}\exp\left\{-\frac{1}{2}\left[\frac{\epsilon_p - \epsilon_N}{s_N}\right]^2\right\}\dot{\epsilon}_p \qquad (4)$$

with f_N the volume fraction of void nucleating particles, and s_N and ϵ_N the standard deviation and the mean of nucleating strain respectively. This approach assumes that the void nucleation process is described by a Gaussian distribution, centered around ϵ_N. The void growth rate can be derived from volume conservation:

$$\dot{f}_{growth} = (1 - f)\dot{\epsilon}^p_{kk} \qquad (5)$$

with $\dot{\epsilon}^p_{kk}$ the trace of the plastic strain rate tensor.

To model HE, the equations above should be adapted to take into account the detrimental effect of the local hydrogen concentration on the macromechanical behavior. In the context of the HELP mechanism, Yu et al. proposed to accelerate the void growth process as a function of the local hydrogen concentration [6]. By accelerating the void growth process, accelerated

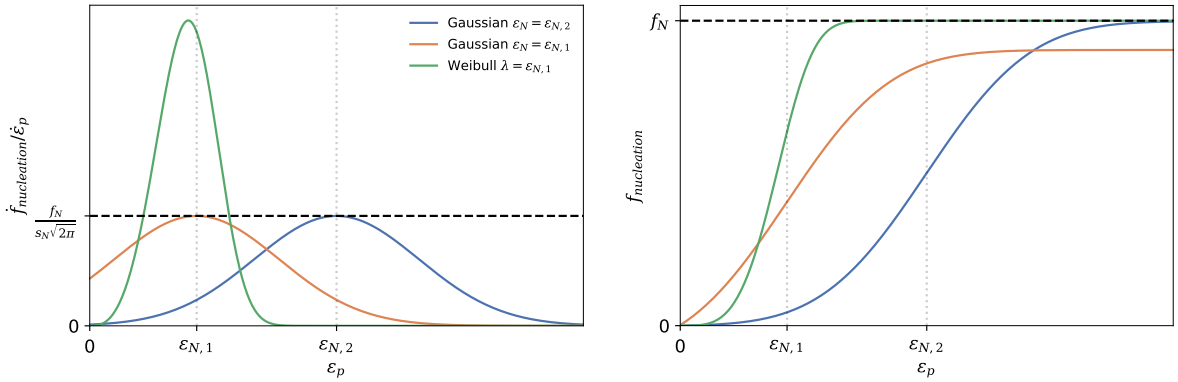

(a) **(b)**

Figure 1: (a) The rate of void nucleation per strain increment, for mean nucleation strains close to zero, with (b) the total void volume fraction resulting from nucleation, which is obtained by integrating (a).

failure is obtained. An alternative to model the HELP mechanism is to adapt the void nucleation equation. Since experiments showed that the presence of hydrogen reduces the local strain at which voids can be observed [14, 15], a reduction of the mean nucleating strain ϵ_N due to a local hydrogen concentration seems an obvious choice. This approach is considered to be more suitable for a metallography-based calibration compared to the approach of Yu et al., since the void nucleating strain can be directly derived from metallographic investigations [14, 16].

Adopting a reduction in the mean nucleating strain ϵ_N in Eq. 4 would lead to bizarre results, since for a very small ϵ_N compared to s_N, a large part of the normal distribution would be negative. Since negative strains are irrelevant, the total amount of voids nucleated at complete failure would not reach f_N. Figure 1 illustrates this concept, indicating the issue when the mean nucleating strain $\epsilon_{N,1}$ approaches zero.

Therefore, this work adopts a Weibull distribution for void nucleation since this distribution features only positive values. Consequently, Eq. 4 is modified to:

$$\dot{f}_{nucleation} = f_N \frac{k}{\lambda} \left(\frac{\epsilon_p}{\lambda}\right)^{k-1} \exp\left\{-\left(\frac{\epsilon_p}{\lambda}\right)^{k}\right\} \dot{\epsilon}_p \tag{6}$$

where $k > 0$ is the shape parameter and $\lambda > 0$ is the scale parameter. The scale parameter λ will approximate the median value of the distribution for large values of k. As such, it has a similar role as the mean parameter ϵ_N in Eq. 4. A Weibull distribution with small λ is shown in Figure 1. To simulate voids nucleating at lower strains due to the local hydrogen concentration C_L, following equation is employed in the current work:

$$\lambda = \frac{\lambda_{C_L=0}}{1 + \xi * C_L} \tag{7}$$

with $\lambda_{C_L=0}$ the scale parameter of the Weibull distribution for the material without any lattice hydrogen, and ξ representing the degradation sensitivity (1/wppm). The equations above are implemented in an Abaqus user material subroutine (UMAT), as described in Depraetere et al. [7].

3 SINGLE EDGE NOTCHED TENSION MODEL

3.1 Geometry and mechanical boundary conditions

The mesh, dimensions and boundary conditions of the SENT specimen employed in this work are presented in Figure 2. Side-grooves are modeled resulting in a 10% total thickness reduction (5% at each side), for the sake of promoting uniform crack growth.

An initial notch is modeled by deleting a single row of elements up to an initial length $a_0 =$ 3mm. One end surface is held fixed while the other surface is given a certain displacement rate $\dot{q}$ [mm/s]. The mesh near the notch consists of cubic three-dimensional linear elements (C3D8T), with a fixed element length of 0.2mm. Only one half of the specimen is modeled because of symmetry.

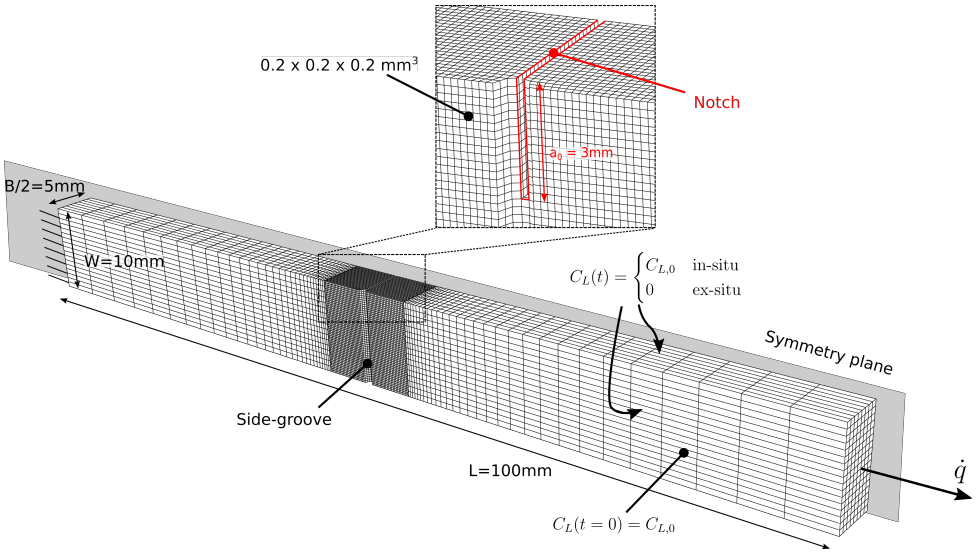

Figure 2: Mesh, dimensions and boundary conditions employed in the SENT toughness test simulations.

3.2 Hydrogen-charging boundary conditions

An accurate implementation of the hydrogen-related boundary conditions is essential to model laboratory toughness tests. In case of an ex-situ test, the surface during mechanical loading is exposed to the atmosphere. This phenomenon is idealized in the model by setting the lattice hydrogen concentration at the surface equal to zero, allowing the hydrogen to effuse out of the specimen. On the other hand, during an in-situ test, the surface is exposed to an active hydrogen environment. To model this, a certain non-zero lattice hydrogen concentration is set at the surface.

It has to be noted that these boundary conditions are idealizations where stress states and surface kinetics are neglected. First of all, the local hydrostatic stress at the edge will affect the boundary condition [17]. Furthermore, the surface will not immediately have the specified hydrogen concentration in reality. Tadashi et al. [18] proposed to implement the equivalent of

Newton's law of cooling as a boundary condition, for a more accurate representation of the surface reactions. This equation however introduces new parameters, requiring more experimental data.

Since the goal of the present work is to model toughness tests featuring an extending crack, newly exposed surface will be created during the simulation. Consequently, the boundary condition has to be updated upon crack extension. This is implemented in Abaqus by transferring the nodes of the failed elements to a multi-point constraint (MPC) subroutine that is responsible for activating the boundary condition on the newly exposed surface, similar to the implementation by Del Busto et al. [19].

Figure 2 displays the hydrogen-charging boundary conditions. The specimen is given a constant initial lattice hydrogen concentration $C_{L,0} = 0.36$ wppm. The boundary condition at the free surface is given as $C_L = C_{L,0}$ for the in-situ simulations, and $C_L = 0$ for the ex-situ simulations.

3.3 Material properties

The flow curve of the considered API 5L X70 steel grade is presented in Figure 3, and was derived from experimental tensile test results. Post-necking characteristics were obtained by recording the diameter contraction during the test, from which the true strain can be determined. Table 1 presents the mechanical and hydrogen-diffusion related parameters employed in the simulations. All material parameters were either determined from experiments, or adopted from literature. In particular, parameters f_0 and f_N were determined by numerical calibration using (notched) round bar tensile experiments on specimens free of hydrogen. The Weibull distribution parameters k and $\lambda_{C_L=0}$ were chosen such that the distribution approximates a Gaussian void nucleation (Eq. 4) with the commonly employed parameters $\epsilon_N = 0.3$ and $s_N = 0.1$.

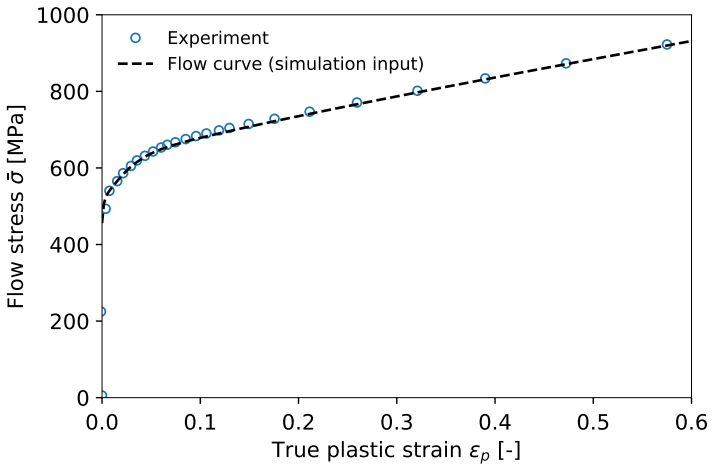

Figure 3: Flow stress $\bar{\sigma}$ versus true plastic strain ϵ_p adopted for the simulations for the API 5L X70 steel. The experimentally obtained data is also shown.

Table 1: Material properties employed. The "exp" stands for experimentally determined.

Gurson			*Hydrogen diffusion*		
Property	**Value**	**Source**	**Property**	**Value**	**Source**
k	3.767	*	D_L	$4.5 \times 10^{-4}\,\mathrm{mm}^2/\mathrm{s}$	exp
$\lambda_{C_L=0}$	0.332	*	E_B	$-30\,\mathrm{kJ/mol}$	[20]
f_N	0.0167	exp	N_L	$8.47 \times 10^{28}\,\mathrm{m}^{-3}$	[20]
f_0	0.00012	exp	N_T	$10^{23.26-2.33\exp(-5.5\epsilon_p)}$	[21]
f_f	0.31	exp	α	1	[20]
q_1	1.42	[22]	β	6	[20]
q_2	0.96	[22]	T	300 K	

*Chosen to approximate the Gaussian distribution in [7]

3.4 Determination of tearing resistance curve

In this study, SENT tearing resistance curves are characterized by means of the Crack Tip Opening Displacement (CTOD) versus the stable crack extension (Δa). CTOD is determined using the relative displacement between the nodes at either side of the crack front, and summing the elastic and plastic component following BS8571 [23]. The crack growth Δa is determined based on the projected area of the failed elements at mid-thickness. Prior to tearing initiation, an additional blunting term estimated as CTOD/2 is added to the crack growth [11]. The initiation toughness can be obtained at the intersection between the tearing resistance curve, and a 0.2mm offset line [24].

4 SINGLE EDGE NOTCHED TENSION (SENT) RESULTS

4.1 Effect of hydrogen degradation sensitivity

By varying the hydrogen degradation sensitivity parameter ξ (Eq. 7), different degrees of embrittlement have been simulated. Figure 4a presents the smoothed crack growth resistance curves for $\xi = 0, 0.5, 2$ and 10 where $\xi = 0$ represents zero degradation, serving as a reference. Of all considered values, the degradation $\xi = 2$ was found to correspond best to the degradation observed in hydrogen-charged (notched) tensile tests of the considered X70 steel, corresponding to a comparable initial hydrogen concentration $C_{L,0} = 0.36$ wppm. In-situ charging boundary conditions together with a displacement rate of $\dot{q} = 0.002$mm/s are applied.

It is clear that by decreasing the mean nucleating strain, increasing toughness reductions can be simulated. The local void volume fraction due to nucleation, $f_{nucleation}$, is extracted for the center element in front of the crack tip (Figure 4b). This corresponds to the integration of Eq. 6.

Figure 5 shows the crack extension for a constant CTOD = 1.5mm and different hydrogen degradation sensitivities. Note that because of symmetry reasons, only one half of the specimen is displayed. The sidegrooves are at the left of each image, while the symmetry plane is at the right. It can be seen that for a constant CTOD, adding hydrogen degradation leads to more crack

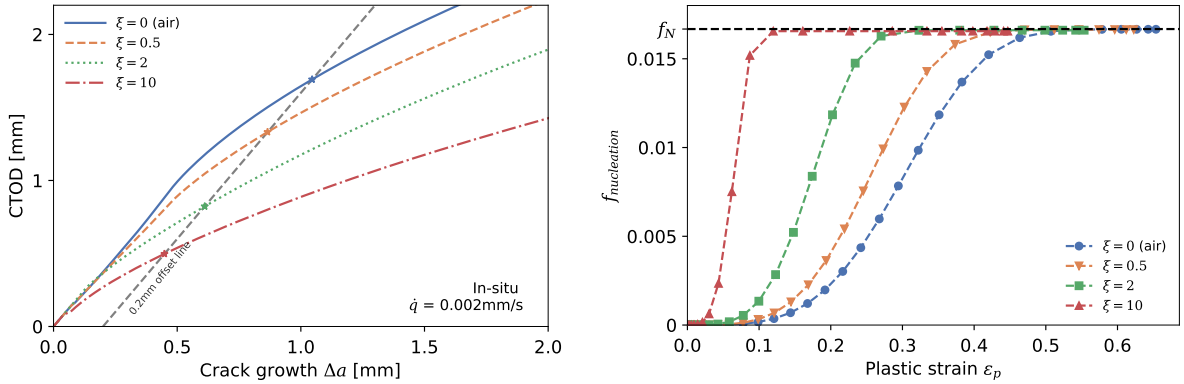

Figure 4: Simulation results of in-situ hydrogen-charged SENT toughness tests with different hydrogen degradation sensitivities ξ, in terms of (a) global resistance curves and (b) the local void volume fraction $f_{nucleation}$ of the center element in front of the crack tip.

propagation. Also, even though side-grooves were modeled, there is still crack non-uniformity, commonly referred to as 'crack tunneling'.

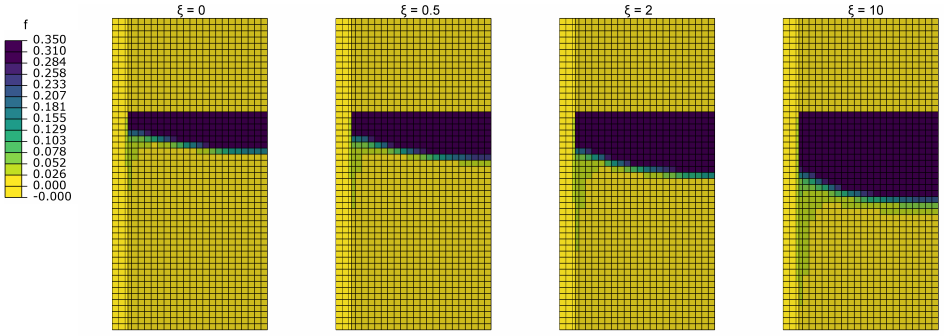

Figure 5: Contour plot showing the void volume fraction f for a fixed CTOD = 1.5mm for various hydrogen degradation sensitivities ξ.

4.2 Effect of hydrogen charging method

To illustrate the effect of in-situ versus ex-situ hydrogen charging, simulations have been performed for $\xi = 2$ with a displacement rate of $\dot{q} = 0.002$mm/s. The resulting crack growth resistance curves are reported in Figure 6a.

As expected, the employed charging method influences the fracture toughness of a hydrogen-charged SENT specimen. Since during ex-situ charging, the freshly created crack surface is immediately assigned a hydrogen concentration of zero, the hydrogen content in the fracture process zone is reduced, leading to a reduction in degradation. Figure 6b shows the hydrogen content along the center path for the ex-situ and in-situ simulations, for three different levels of

CTOD. The growing crack results in a rightward shift of the curve. Just in front of the crack tip, an increased hydrogen concentration as a result of the stress-assisted diffusion is apparent. It is also clear that the in-situ tests result in a higher hydrogen concentration near the crack tip. The difference between ex-situ and in-situ hydrogen charging is the direct effect of the trade-off between the process of hydrogen diffusion that is characterized by the diffusion coefficient D_L, and the crack propagation speed, which is an output of the displacement rate $\dot{q}$. The next section will explore the effect of displacement rate on tearing resistance behaviour.

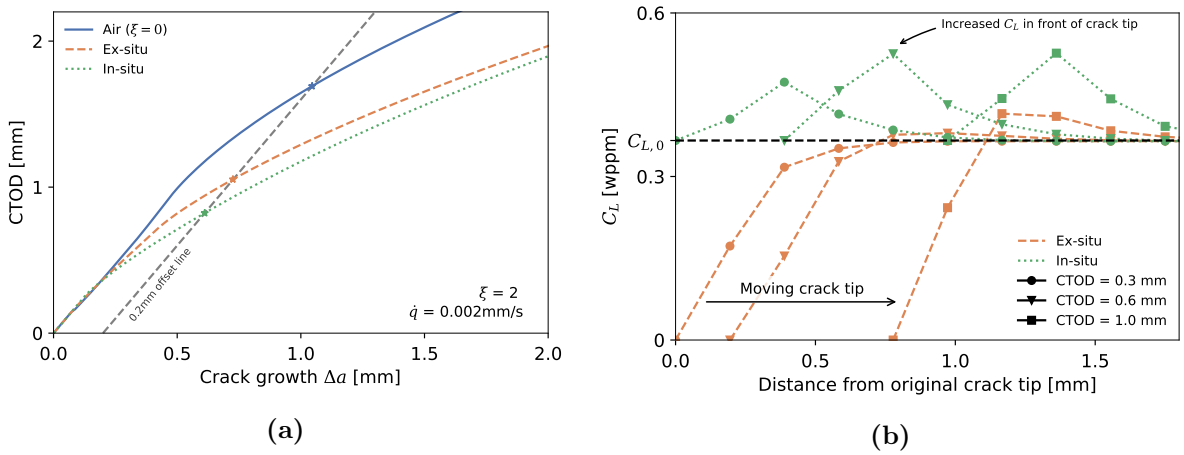

Figure 6: Simulation results of ex-situ and in-situ hydrogen-charged SENT toughness tests with $\xi = 2$, in terms of (a) global resistance curves and (b) the lattice hydrogen concentration C_L along a path starting from the original crack tip, for three different levels of CTOD.

4.3 Effect of displacement rate

Since the displacement rate is an important parameter in the dynamics between hydrogen diffusion and crack propagation, various displacement rates have been simulated: $\dot{q} = 2 * 10^{-5}, 0.002$ and 0.2mm/s. A degradation factor $\xi = 2$ is employed. Figure 7 presents the smoothed resistance curves for (a) ex-situ charging and (b) in-situ charging.

When the displacement rate is large compared to the process of hydrogen diffusion, there is no effect of hydrogen diffusion. Both the ex-situ and in-situ simulation are equivalent and show the toughness reduction with a constant hydrogen concentration $C_L = C_{L,0}$. By applying a slower displacement rate, however, different trends develop for ex-situ and in-situ charging. A slow displacement rate during ex-situ charging leads to all hydrogen effusing, resulting in a crack growth resistance curve similar to the reference one ($\xi = 0$). On the contrary, for in-situ charging, a slower displacement rate allows the hydrogen concentration near the crack tip to approach a steady-state, resulting in an increased fracture toughness degradation. Further analysis shows that a displacement speed $\dot{q} = 2 * 10^{-5}$mm/s leads to steady-state results, for the employed parameters (Table 1).

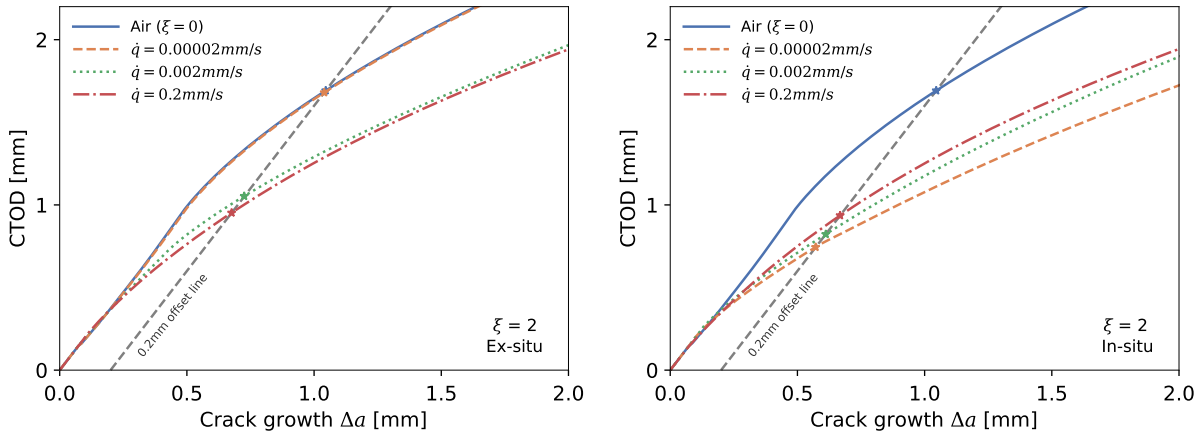

Figure 7: Resistance curves for various displacement speeds for ex-situ and in-situ toughness tests

5 CONCLUSIONS

Hydrogen embrittlement has been modeled using a Gurson damage model, by reducing the mean void nucleating strain, depending on the local hydrogen concentration C_L. Hereby, void nucleation is described by a Weibull distribution, instead of the conventional Gaussian distribution since the former applies to strictly positive values of applied strain. Finite element simulations of Single Edge Notched Tension (SENT) tests were employed to investigate the influences of two test parameters on tearing resistance behaviour: (a) ex-situ versus in-situ charging conditions, and (b) deformation rate.

By decreasing the mean void nucleating strain, toughness reductions can be obtained. This is in agreement with experimental observations that the presence of hydrogen in steel can lead to accelerated void nucleation [14], and leads to a decrease in toughness [2]. The effect of in-situ charging versus ex-situ charging on the tearing resistance is strongly dependent on the displacement speed. If the process of crack propagation would be too slow compared to the mechanism of diffusion, no toughness reductions are observed in the case of ex-situ charging due to hydrogen effusion. In the case of in-situ charging conditions, however, a slower displacement rate will yield a larger reduction in toughness.

In order to evaluate conservative and trustworthy toughness reductions due to hydrogen, in-situ experimental testing is advised. Before the test, it should be assessed whether the chosen displacement rate is slow enough to ensure that the hydrogen concentration in front of the crack tip is near steady-state, resulting in conservative results. In future work, the numerically observed effects will be compared to test results.

REFERENCES

[1] The American Society of Mechanical Engineers, Hydrogen Piping and Pipelines (ASME B31.12:2019), 2019.

[2] M. B. Djukic, G. M. Bakic, V. Sijacki Zeravcic, A. Sedmak, B. Rajicic, The synergistic

action and interplay of hydrogen embrittlement mechanisms in steels and iron: Localized plasticity and decohesion (2019). doi:10.1016/j.engfracmech.2019.106528.

[3] S. P. Lynch, Hydrogen embrittlement (HE) phenomena and mechanisms, Stress corrosion cracking: Theory and practice (i) (2011) 90–130. doi:10.1533/9780857093769.1.90.

[4] G. Gobbi, C. Colombo, S. Miccoli, L. Vergani, A fully coupled implementation of hydrogen embrittlement in FE analysis, Advances in Engineering Software 135 (July) (2019) 102673. doi:10.1016/j.advengsoft.2019.04.004.

[5] A. H. Krom, R. W. Koers, A. Bakker, Hydrogen transport near a blunting crack tip, Journal of the Mechanics and Physics of Solids 47 (4) (1999) 971–992. doi:10.1016/S0022-5096(98)00064-7.

[6] H. Yu, J. S. Olsen, A. Alvaro, L. Qiao, J. He, Z. Zhang, Hydrogen informed Gurson model for hydrogen embrittlement simulation, Engineering Fracture Mechanics 217 (February) (2019) 106542. doi:10.1016/j.engfracmech.2019.106542.

[7] R. Depraetere, W. De Waele, S. Hertelé, Fully-coupled continuum damage model for simulation of plasticity dominated hydrogen embrittlement mechanisms, Computational Materials Science 200 (2021) 110857. doi:10.1016/j.commatsci.2021.110857.

[8] M. Lin, H. Yu, Y. Ding, G. Wang, V. Olden, A. Alvaro, J. He, Z. Zhang, A predictive model unifying hydrogen enhanced plasticity and decohesion, Scripta Materialia 215 (2022) 114707. doi:10.1016/j.scriptamat.2022.114707.

[9] M. Asadipoor, J. Kadkhodapour, A. Pourkamali Anaraki, S. M. Sharifi, A. C. Darabi, A. Barnoush, Experimental and Numerical Investigation of Hydrogen Embrittlement Effect on Microdamage Evolution of Advanced High-Strength Dual-Phase Steel, Metals and Materials International (0123456789) (2020). doi:10.1007/s12540-020-00681-1.

[10] G. G. Youn, Y. J. Kim, J. S. Kim, P. S. Lam, A Fracture Strain Based Numerical Prediction Method For Hydrogen Effect on Fracture Toughness, International Journal of Mechanical Sciences 202-203 (2021) 106492. doi:10.1016/J.IJMECSCI.2021.106492.

[11] M. A. Verstraete, R. M. Denys, K. Van Minnebruggen, S. Hertelé, W. De Waele, Determination of CTOD resistance curves in side-grooved Single-Edge Notched Tensile specimens using full field deformation measurements, Engineering Fracture Mechanics 110 (2013) 12–22. doi:10.1016/j.engfracmech.2013.07.015.

[12] Z. L. Zhang, C. Thaulow, J. Ødegård, Complete Gurson model approach for ductile fracture, Engineering Fracture Mechanics 67 (2) (2000) 155–168. doi:10.1016/S0013-7944(00)00055-2.

[13] C. C. Chu, A. Needleman, Void nucleation effects in biaxially stretched sheets, Journal of Engineering Materials and Technology, Transactions of the ASME 102 (3) (1980) 249–256. doi:10.1115/1.3224807.

[14] D. I. Kwon, R. J. Asaro, Hydrogen-assisted ductile fracture in spheroidized 1518 steel, Acta Metallurgica Et Materialia 38 (8) (1990) 1595–1606. doi:10.1016/0956-7151(90)90127-3.

[15] T. Matsuo, N. Homma, S. Matsuoka, Y. Murakami, Effect of Hydrogen and Prestrain on Tensile Properties of Carbon Steel SGP (0.078 C-0.012 Si-0.35 Mn, mass%) for 0.1 MPa Hydrogen Pipelines, Nihon Kikai Gakkai Ronbunshu, A Hen/Transactions of the Japan Society of Mechanical Engineers, Part A 74 (744) (2008) 1164–1173. doi:10.1299/kikaia.74.1164.

[16] P. Verleysen, J. Peirs, Quasi-static and high strain rate fracture behaviour of Ti6Al4V, International Journal of Impact Engineering 108 (2017) 370–388. doi:10.1016/j.ijimpeng.2017.03.001.

[17] A. Díaz, I. I. Cuesta, C. Rodríguez, J. M. Alegre, Influence of non-homogeneous microstructure on hydrogen diffusion and trapping simulations near a crack tip in a welded joint, Theoretical and Applied Fracture Mechanics 112 (apr 2021). doi:10.1016/j.tafmec.2020.102879.

[18] K. Tadashi, A. Y. Toshimitsu, O. Go, O. Toshihito, E. Manabu, Modelling of hydrogen diffusion in a weld cold cracking test: Part 1, experimental determinations of apparent diffusion coefficient and boundary condition, ISIJ International 61 (4) (2021) 1245–1253. doi:10.2355/isijinternational.ISIJINT-2020-523.

[19] S. del Busto, C. Betegón, E. Martínez-Pañeda, A cohesive zone framework for environmentally assisted fatigue, Engineering Fracture Mechanics (2017). arXiv:1711.09965, doi:10.1016/j.engfracmech.2017.05.021.

[20] L. Jemblie, V. Olden, O. M. Akselsen, A coupled diffusion and cohesive zone modelling approach for numerically assessing hydrogen embrittlement of steel structures, International Journal of Hydrogen Energy 42 (16) (2017) 11980–11995. doi:10.1016/j.ijhydene.2017.02.211.

[21] A. J. Kumnick, H. H. Johnson, Deep trapping states for hydrogen in deformed iron, Acta Metallurgica 28 (1) (1980) 33–39. doi:10.1016/0001-6160(80)90038-3.

[22] J. Faleskog, X. Gao, C. Fong Shih, Cell model for nonlinear fracture analysis - I. Micromechanics calibration, International Journal of Fracture 89 (4) (1998) 355–373. doi:10.1023/A:1007421420901.

[23] The Britisch Standards Institution, Method of test for determination of fracture toughness in metallic materials using single edge notched tension (SENT) specimens (BS8571:2018), 2018.

[24] American Society for Testing and Materials, Standard Test Method for Measurement of Fracture Toughness (ASTM E1820 - 20a).